ACS OMEGA

Open Access

This article is licensed under CC-BY-NC-ND 4.0

http://pubs.acs.org/journal/acsodf

Article

Nitrogen Defect-Rich Graphitic Carbon Nitride for Highly Sensitive Voltammetric Determination of Tryptophan

Yeabsira Mihret, Getu Sisay, Abebe Diro, Solomon Hailemariam, and Shimeles Addisu Kitte*

Cite This: *ACS Omega* 2023, 8, 46869−46877

Read Online

ACCESS | Metrics & More | Article Recommendations | Supporting Information

ABSTRACT: Here, a highly sensitive electrochemical sensor for detection of tryptophan (Trp) using a nitrogen defect graphitic carbon nitride-modified glassy carbon electrode (ND-CN/GCE) was introduced. ND-CN/GCE showed a higher oxidation current for Trp than the graphitic carbon nitride-modified glassy carbon electrode (*g*-CN/GCE) and bare glassy carbon electrode (BGCE). The synthesized nitrogen defect-rich graphitic carbon nitride (ND-CN) was characterized using X-ray photoelectron spectroscopy, X-ray diffraction spectroscopy, Fourier-transform infrared spectroscopy, scanning electron microscopy, and transmission electron microscopy. Electrochemical impedance spectroscopy and cyclic voltammetry were used to further analyze the electrochemical properties of BGCE, *g*-CN/GCE, and ND-CN/GCE. The oxidation of Trp at ND-CN/GCE is a diffusion-controlled process at pH 3.0. It was calculated that the transfer coefficient, rate constant, and diffusion coefficient of Trp were 0.53, 2.24×10^3 M^{-1} s^{-1}, and 8.3×10^{-3} cm^2 s^{-1}, respectively, at ND-CN/GCE. Trp was detected using square wave voltammetry, which had a linear range from 0.01 to 40 μM at pH 3.0 and a limit of detection of about 0.0034 μM ($3\sigma/m$). Analyzing the presence of Trp in a milk and multivitamin tablet sample with a percentage recovery in the range of 97.0−108% satisfactorily demonstrated the practical usability of the electrochemical sensor. The ND-CN/GCE additionally displays good repeatability and reproducibility and satisfactory selectivity.

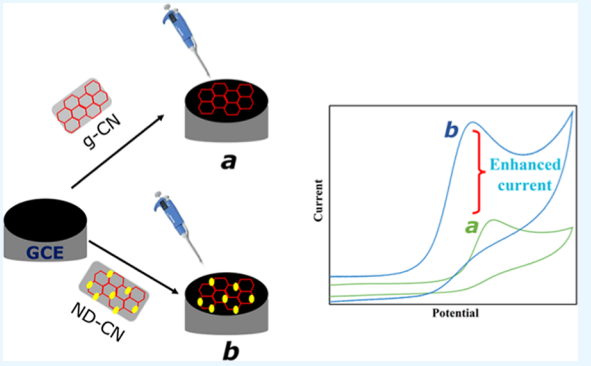

INTRODUCTION

Tryptophan (Trp) is an essential amino acid with nutritional and medical importance and only available to humans through dietary consumption of food products or pharmaceutical preparations.[1] Trp and its metabolites, particularly serotonin, are crucial for the production of proteins as well as other bodily functions, such as neurotransmission, signaling, and the control of sleep and mood,[2] essential for maintaining an adequate amount of nitrogen in the body.[3] The Trp level can also be used as a tool for clinical diagnosis to identify various metabolic problems and the symptoms associated with them.[4] On the other hand, Trp has some moderate or serious side effects to humans, such as tiredness, loss of appetite, and accumulation of toxic substances in the brain.[1] As recommended by the World Health Organization, adults should consume 4 mg/kg of Trp each day.[5] Therefore, simple, accurate, and sensitive methods for determining Trp are highly required to detect Trp in food, biological systems, and pharmaceutical formulations. Numerous techniques have been developed to determine Trp such as high-performance liquid chromatography,[6] electrochemiluminescence,[7] capillary electrophoresis,[8] and electrochemical sensors.[9]

Sensitive detection of important biomolecules, such as Trp, is essential in pharmaceutical and biological samples. Since these kinds of biomolecules exist in low concentrations, sensitive biosensors should be developed. Hence, electrochemical sensors provide quick, exact, sensitive, selective, and simple-to-use analytical techniques.[10]

Two-dimensional (2D) nanomaterials are the thinnest nanomaterials with the largest surface area to volume ratio, which helps to achieve the maximum efficiency. Chemical stability and biocompatibility are some of the special qualities that 2D nanomaterials possess. Consequently, they are appropriate for a variety of sensor applications.[11] Graphitic carbon nitride (*g*-CN) is one of the attractive 2D materials with carbon−nitrogen bonds. The presence of the nitrogen atom increases catalytic electron transfer, making it a suitable 2D nanomaterial for electrochemical sensors that may be utilized to detect a variety of substances.[12] For instance, it has been used for voltammetric toxic heavy metals' detection,[13] organic pollutants,[14] pharmaceuticals,[15] biomolecules,[16] food additives,[17] and so on. Researchers have recently made

Received: August 30, 2023
Revised: November 9, 2023
Accepted: November 14, 2023
Published: November 30, 2023

© 2023 The Authors. Published by American Chemical Society

numerous attempts to improve the catalytic activities of *g*-CN, such as by making nanocomposite materials with metal nanoparticles, carbon compounds, and metal oxides.[18] Another method for increasing the catalytic property of *g*-CN is to introduce defects into its structure.[19] Therefore, experimental findings revealed that a superior electrochemical performance of *g*-CN can be attained by surface modification via the introduction of defects in its structure.[20] It was reported that defect-containing *g*-CN showed superior electrochemical activity than *g*-CN because it can considerably alter the electronic structure and speed up interfacial electron transfer.[21,22]

Defect-containing *g*-CN has been widely studied in catalysis and photocatalysis. Niu et al. synthesized nitrogen defect-rich graphitic carbon nitride (ND-CN) and examined its photocatalytic activity. They revealed improved photocatalytic activity for Rhodamine B photodecomposition and the evolution of hydrogen from water splitting.[23] Yuan and coworkers synthesized defect-containing *g*-CN and found 5 times higher photocatalytic hydrogen evolution reaction than for *g*-CN.[24] There are also some good efforts made to improve the catalytic activity of *g*-CN using introduction of defects.[25] Still, the significance of defects in the structure of *g*-CN on electrochemical sensor development has been neglected.

In this study, the detection of Trp using an ultrathin ND-CN nanosheet (NS)-based voltammetric sensor was demonstrated. By thermally polymerizing *g*-CN under inert conditions, ND-CN was produced and used for modifying GCE. A comparison was made between bare glassy carbon electrode (BGCE), graphitic carbon nitride-modified glassy carbon electrode (*g*-CN/GCE) and nitrogen defect graphitic carbon nitride-modified glassy carbon electrode (ND-CN/GCE) toward oxidation of Trp. It was found that ND-CN/GCE exhibited superior electrocatalytic oxidation, enhanced anodic peak current, and less overpotential toward Trp as compared to *g*-CN/GCE and BGCE. Furthermore, the suggested electrode showed excellent repeatability, reproducibility, and a low detection limit. Trp in a milk sample was successfully determined using the produced ND-CN/GCE. The approach used in this study can also be used for other electroactive compounds.

EXPERIMENTAL SECTION

Chemicals. Urea (CH_4N_2O, 99%) was obtained from Alfa Aesar Chemical Reagent, China. Trp ($C_{11}H_{12}N_2O_2$, 99.9%) was purchased from Sinopharm Chemical Reagent, China. Phosphoric acid (H_3PO_4, 85%) was obtained from Riedel de Haen, Germany. Potassium chloride (KCl, 99.8%), potassium dihydrogen phosphate (KH_2PO_4, 99.5%), and potassium phosphate dibasic (K_2HPO_4, 99%) were obtained from Aladdin Reagents, China. Sodium hydroxide (NaOH, 98%) was bought from Shanghai Chemical Reagent, China. Potassium ferricyanide ($K_3[Fe(CN)_6]$, 99%) and potassium ferrocyanide ($K_4[Fe(CN)_6]$, 99%) were bought from NICE Chemical Reagent, India. All of the aqueous solutions were made with double-distilled water.

Apparatus. Electrochemical studies were conducted using the Epsilon EC-Ver 1.40.67, Bioanalytical System and the CHI 800B, Chenhua Instruments. The X-ray diffraction (XRD) patterns for *g*-CN and all of the ND-CNs were obtained using the D8 ADVANCE X-ray diffractometer (Bruker, Germany) with Cu Kα radiation = 1.54 A°. The Thermo ESCALAB 250XI (Thermo Fisher, USA) X-ray photoelectron spectroscopy (XPS) instrument was utilized for the analysis of elements. To determine the size and shape of the produced materials, the JEM-2100F transmission electron microscopy (TEM) instrument was used. The NICOLET iS50 Fourier-transform infrared (FT-IR) spectroscopy instrument was used to study the functional groups in the synthesized materials. Three electrodes were used during the electrochemical tests. The working electrodes were BGCE, *g*-CN/GCE, and ND-CN550/GCE, the reference electrode was Ag/AgCl (saturated KCl), and the auxiliary electrode was Pt wire. A solution of 0.1 M KCl containing 1 mM $[Fe(CN)_6]^{3-/4-}$ was used for the electrochemical impedance spectroscopy (EIS) experiments.

Synthesis of *g*-CN. Ten grams of urea was placed in a crucible and heated at a rate of 5 °C per minute in a muffle furnace to 500 °C and maintained at this temperature for 2 h. A yellow colored *g*-CN was produced after being cooled to room temperature.[26] It was then crushed and stored until needed.

Synthesis of ND-CN. Separate crucibles containing 2 g of *g*-CN were heated in a furnace under inert conditions to temperatures of 500, 550, and 600 °C at a rate of 5 °C/min, and the temperature was then maintained for 2 h at each respective temperature.[22] Lastly, the powders were given the names ND-CN500, ND-CN550, and ND-CN600.

***g*-CN and ND-CN NS Preparation.** The thin NSs of the synthesized *g*-CN and ND-CNs were made by dispersing 100 mg of *g*-CN and ND-CNs powder in 100 mL of water and ultrasonically processing it overnight. The dispersed solution was then centrifuged to remove the residue and large *g*-CN NS and ND-CN NS particles. The supernatant was then saved for electrode modification.[22]

***g*-CN/GCE and ND-CN/GCE Preparation.** GCE was polished using an alumina slurry of 0.3 and 0.05 m, sonicated, and then washed with double-distilled water. Following that, 10 μL of *g*-CN and each ND-CN NSs were placed on GCE and allowed to dry at room temperature. When the electrodes were not in use, we kept the modified electrodes in the refrigerator at 4 °C. The anodic current of Trp of each electrode was then measured to select the optimal ND-CN NSs.

Sample Preparation. Ten mM Trp (10 mM) was prepared in double-distilled water and kept in the refrigerator for later use. On the day of the experiment, a working solution of Trp was made by diluting a needed amount of Trp stock solution in 0.1 M phosphate buffer solution (PBS) with a pH of 3.0.

Real Sample Analysis. The practical applicability of ND-CN550/GCE was assessed by using it for the detection of Trp in a cow milk sample and multivitamin tablets. The content of Trp was determined using a standard addition method. The milk was filtered without any prior treatment and then diluted five times in 0.1 M PBS with a pH of 3.0. Then, 1, 5, and 10 μM Trp were spiked in the milk sample and analyzed under the optimized experimental conditions using square wave voltammetry (SWV). Multivitamin tablets (EPHAVIT Multivitamin Tablets, Ethiopian Pharmaceuticals Manufacturing Sc.) were purchased from a local pharmacy in Jimma town, Ethiopia. Then, the tablets were ground to a fine powder and dissolved in double-distilled water. After that, the mixture was centrifuged for 10 min to remove undissolved particles if any. Finally, the supernatant solution was taken, and the pH was adjusted to pH 3.0 with PBS. Then, 1, 5, and 10 μM Trp were spiked and analyzed using SWV.

https://doi.org/10.1021/acsomega.3c06487
ACS Omega 2023, 8, 46869−46877

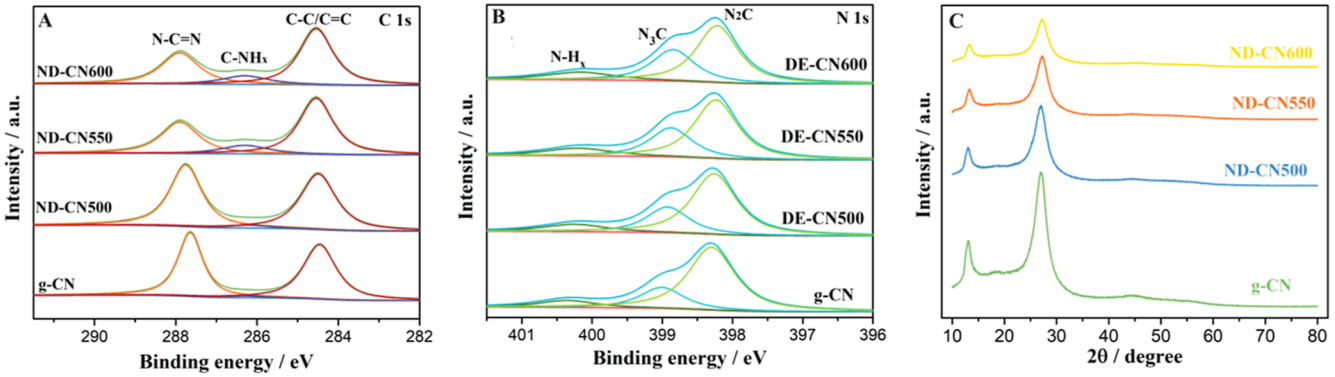

Figure 1. XPS bands of C 1s (A) and N 1s (B), XRD patterns (C), and FT-IR spectra (D) of *g*-CN and different ND-CNs.

RESULTS AND DISCUSSION

Characterization of *g*-CN and ND-CNs. XPS was used to investigate the chemical state of carbon and nitrogen in the produced product. As can be seen in Figure S1, C, N, and O dominate the survey spectrum of *g*-CN, ND-CN500, ND-CN550, and ND-CN600. The C 1s spectra for *g*-CN, ND-CN500, ND-CN550, and ND-CN600 are shown in Figure 1A. The peaks at 288.9, 286.2, and 284.3 eV were assigned for N−C═N, C−NHx, and C−C/C═C, respectively. As the polymerization temperature rises, the peak at 286.5 eV becomes more intense, suggesting the formation of the N═CH−N bonds and the loss of atoms from the $N(C)_2$ group.[27,28] In addition, the N 1s spectra for *g*-CN and ND-CNs at around 400.9 eV are attributed to the N−Hx bonds, 399 eV is attributed to the N−C ($N(C)_3$) bonds, and 398.5 eV is ascribed to the N−C═N ($N(C)_2$) bonds (Figure 1B).[27−29] The ratios of the peak area of $N(C)_2$ to $N(C)_3$ for *g*-CN, ND-CN500, ND-CN550, and ND-CN600 were 4.34, 3.54, 2.82, and 2.43, respectively. As the polymerization temperature rises, the ratio of the peak area of $N(C)_2$ to $N(C)_3$ decreases, which shows that N atoms are being lost during the heat treatment process.[21,27]

In Figure 1C, the XRD patterns of *g*-CN, ND-CN500, ND-CN550, and ND-CN600 are displayed. The (100) in-plane packing and (002) plane represented for *g*-CN interfacial stacking are responsible for the two *g*-CN diffraction peaks that were observed at 13.1 and 27.2°. The XRD spectra for *g*-CN, ND-CN500, ND-CN550, and ND-CN600 (Figure 1C) revealed two distinguishing peaks at 13.0 and 27.3, which resulted from the in-plane packing of the aromatic system and interlayer stacking, respectively. The eventual bond breakdown in the *g*-CN framework is demonstrated by the gradual reduction of these two diffraction peaks when treatment temperature was raised.[30] The structural information on the as-prepared product was also investigated using FT-IR spectroscopy. As shown in Figure S1B, the peaks seen between 3400 and 3000 cm^{-1} are caused by N−H stretching. However, the peak at 800 cm^{-1} was produced by triazine unit out-plane bending. Stretching vibrations of the C−N−C and C═N atoms can be attributed to the smaller peaks from 1750 to 1100 cm^{-1}. In general, the fundamental structure of *g*-CN remained unchanged, even after defects were introduced.

Additionally, scanning electron microscopy (SEM) images revealed that the surfaces of ND-CN500, ND-CN550, and ND-CN600 were rough with numerous pores, in contrast to the surfaces of *g*-CN, showing a change in surface morphology following heating (Figure 2). The resultant *g*-CN and ND-CN NSs were characterized by TEM. The TEM images of the *g*-CN, ND-CN500, ND-CN550, and ND-CN600 NSs reveal a two-dimensional sheetlike structure (Figure S2).

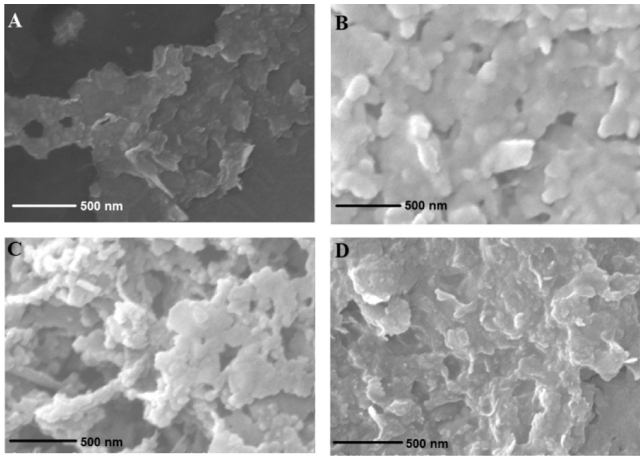

Figure 2. SEM images of *g*-CN (A), ND-CN500 (B), ND-CN550 (C), and ND-CN 600 (D).

Electrochemical Characteristics of BGCE, *g*-CN/GCE, and ND-CN550/GCE. Using cyclic voltammetry (CV) and EIS methods, the electrochemical properties of BGCE and modified GCEs were investigated in a 0.1 M KCl solution containing 1 mM $Fe(CN)_6^{3-/4-}$. As shown in Figure 3A, the $Fe(CN)_6^{3-/4-}$ oxidation and reduction peaks were produced at BGCE, *g*-CN/GCE, and higher than those at *g*-CN/GCE and BGCE because ND-CN550 has a higher conductivity, which enables fast electron transfer at the interface.

CVs of $[Fe(CN)_6]^{3-/4-}$ were recorded at various scan rates ranging from 10 to 100 mV/s on BGCE, *g*-CN/GCE, and ND-CN550/GCE to determine the electrochemical active surface area (EASA) (Figure S3). The EASA values of the electrodes were then calculated using the Randles Sevcik equation for a reversible electrode technique. The following eq (eq 1) describes the peak current (I_p).[31]

$$I_p = 2.69\times10^5 n^{3/2} A D^{1/2} v^{1/2} C \quad (1)$$

where n is the number of electrons participating (n = 1 for $[Fe(CN)_6]^{3-}$), A represents the surface area of the electrodes, D denotes the diffusion coefficient (7.6×10^{-6} cm^2 s^{-1}), v represents the scan rate (V s^{-1}), and C denotes the concentration of $[Fe(CN)_6]^{3-}$ (1×10^{-4} mol cm^{-3}). It was determined that the EASA values of BGCE, *g*-CN/GCE, and ND-CN550/GCE were 0.071, 0.14, and 0.24 cm^2, respectively.

https://doi.org/10.1021/acsomega.3c06487
ACS Omega 2023, 8, 46869−46877

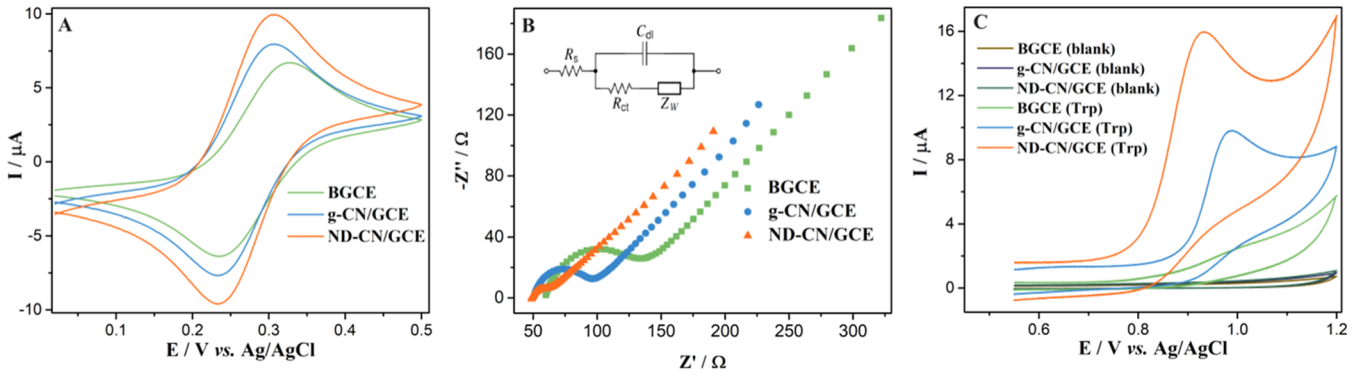

Figure 3. (A) CVs and (B) Nyquist plots of the BGCE, *g*-CN/GCE, and ND-CN550/GCE in 0.1 mM $[Fe(CN)_6]^{3-/4-}$ solution in 0.1 M KCl (inset: randles equivalent circuit diagram). (C) CVs of BGCE, *g*-CN/GCE, and ND-CN550/GCE in 10 μM Trp pH 3.0.

Accordingly, we can conclude that ND-CN550 provided greater EASA because it might contain the highest number of defects compared to the others. Furthermore, the electrochemical properties of BGCE, *g*-CN/GCE, and ND-CN550/GCE were investigated using EIS spectra (Figure 3B). When different substances are attached to the surface of the electrode, the surface properties of the electrode change, resulting in an EIS difference.[32] The EIS spectra consist of a semicircle with a diameter proportional to the resistance to charge transfer (R_{ct}) at high frequencies and a line representing the diffusion-limited process at low frequencies. ND-CN550/GCE exhibits a very small semicircle (~60 Ω), signifying a very low R_{ct}, which is lower than those of *g*-CN/GCE (~100 Ω) and BGCE (~150 Ω). This is due to the great electronic conductivity and rapid electron transfer of ND-CN, which is well-matched with the CV results.

Electrochemical Behavior of Trp at BGCE, *g*-CN/GCE, and ND-CN550/GCE. Figure 3C depicts the CVs of BGCE, *g*-CN/GCE, and ND-CN550/GCE in blank PBS (0.1 M, pH 3.0) and in the presence of Trp (0.1 M, pH 3.0 PBS). All electrodes show no redox peaks in blank PBS (Figure 3C inset). The BGCE has the lowest oxidation current for Trp. The anodic current response of *g*-CN/GCE increased considerably, demonstrating that *g*-CN improves Trp sensing compared to BGCE.

ND-CN550/GCE, on the other hand, has the highest anodic peak current density toward Trp oxidation than *g*-CN/GCE and BGCE. This is due to ND-CN having higher electrochemical activity than *g*-CN because it can significantly accelerate interfacial electron transport. Our results are clearly in line with the results of the EASA and EIS studies.

Amount of ND-CN NSs. The effect of the volume of ND-CN NSs on the Trp oxidation was studied to select the optimum amount of ND-CN NSs, which gives a maximum current response. As depicted in Figure S4, the anodic peak current of Trp increases with an increase in the volume of ND-CN NSs up to 10 μL but further increase in the amount of ND-CN has no significant change in the oxidation current of Trp. Therefore, 10 μL of Trp was used to modify the working electrode.

Effects of pH. The effect of buffer pH on Trp oxidation at ND-CN550/GCE was examined by recording CVs of 10 μM Trp in 0.1 M PBS in the pH range of 2.0−8.0, as shown in Figure 4A,B. It is obvious that the anodic peak currents had an influence as the pH of the buffer solution increased, with the maximum oxidation current for Trp found at pH 3.0. Thus, PBS at pH 3.0 was selected as the optimal pH for detecting

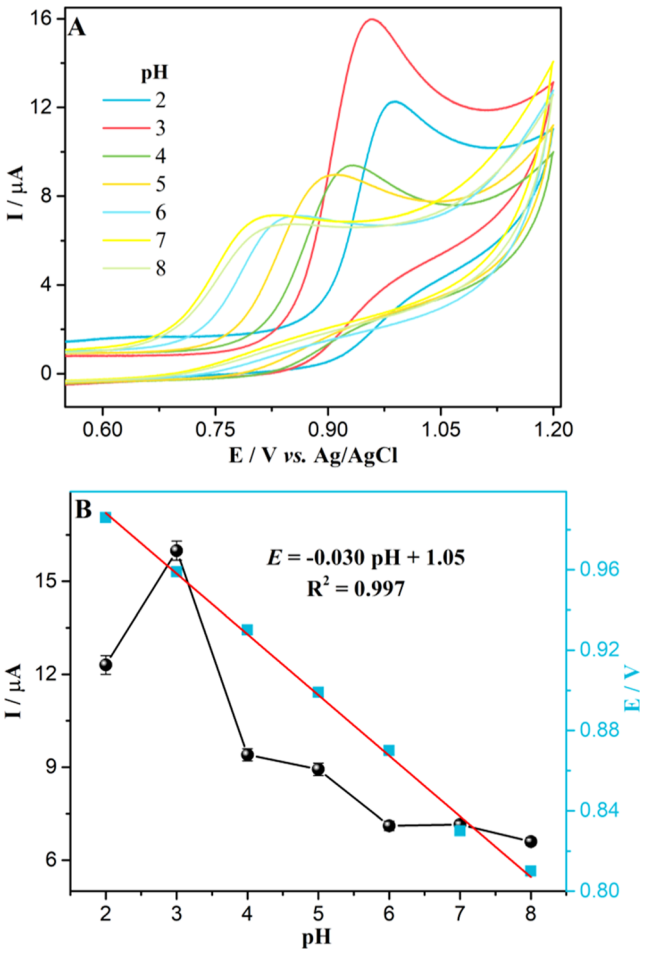

Figure 4. (A) Effect of pH on oxidation of Trp at ND-CN/GCE. (B) Plot of oxidation current and potential of Trp as a function of pH (measurements were made in triplicate, and each point is mean ± SD).

Trp in this study. A change in pH influenced the oxidation potential, as well. With increasing pH, the anodic potential of Trp decreased. This shows that the proton is involved in the oxidation process. The anodic potential of Trp at different pH is directly related to pH, as shown by the equation: E (V) = −0.030pH + 1.05, R^2 = 0.997 (Figure 4B). The obtained slope has a value of 0.030, which is less than the value that is theoretical (0.059) for the $2e^-/2H^+$ involved process. The

https://doi.org/10.1021/acsomega.3c06487
ACS Omega 2023, 8, 46869−46877

Scheme 1. Mechanism of Electrocatalytic Oxidation of Trp at the ND-CN550/GCE

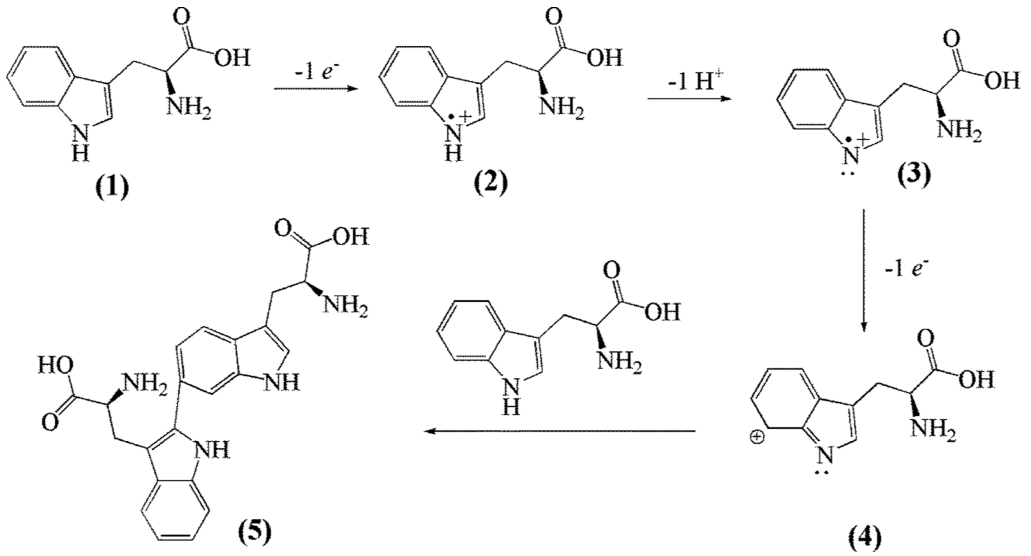

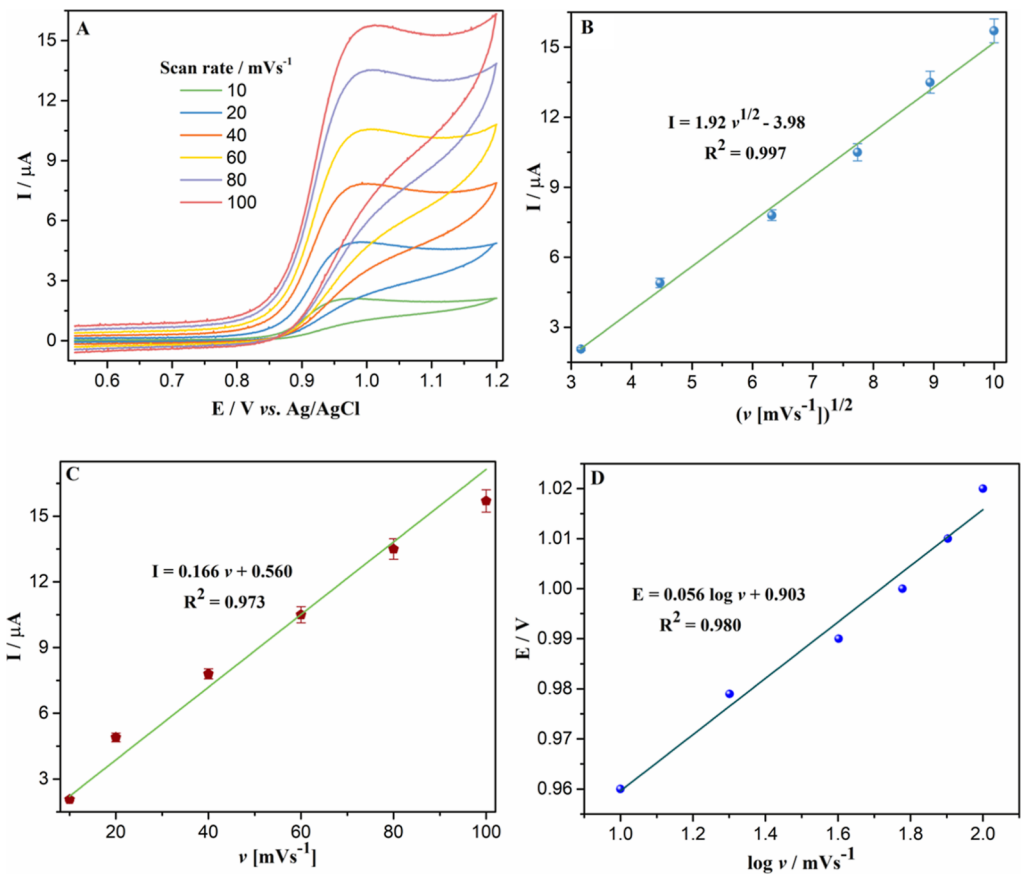

Figure 5. (A) CVs at various scan rates for 10 μM Trp in PBS (pH = 4.0) at ND-CN550/GCE: 10, 20, 40, 60, 80, and 100 mV s^{-1}. (B,C) Plots of the linear relationship between peak currents vs square root of scan rate and peak currents vs scan rate. (D) Plot of log ν vs E (measurements were made in triplicate and each point is the mean ± SD).

obtained slope value was then applied to the Nernst Equation (eq 2).[33]

$$E_p = \frac{-0.0591m}{n}\text{pH} + b \quad (2)$$

where m and n are the protons' and electrons' numbers, respectively. The value of m/n for Trp was determined to be 0.51 by using eq 2. Consequently, the oxidation of Trp at ND-CN550/GCE can be ascribed to the $2e^-/1H^+$ transfer mechanism, as previously reported.[34,35] Scheme 1 depicts the proposed mechanism. During the anodic process of Trp at ND-CN/GCE, the first step comprises the formation of a radical cation by one-electron (1e−) removal [Structure (2) in Scheme 1]. After that, it is further oxidized by the loss of the

https://doi.org/10.1021/acsomega.3c06487
ACS Omega 2023, 8, 46869−46877

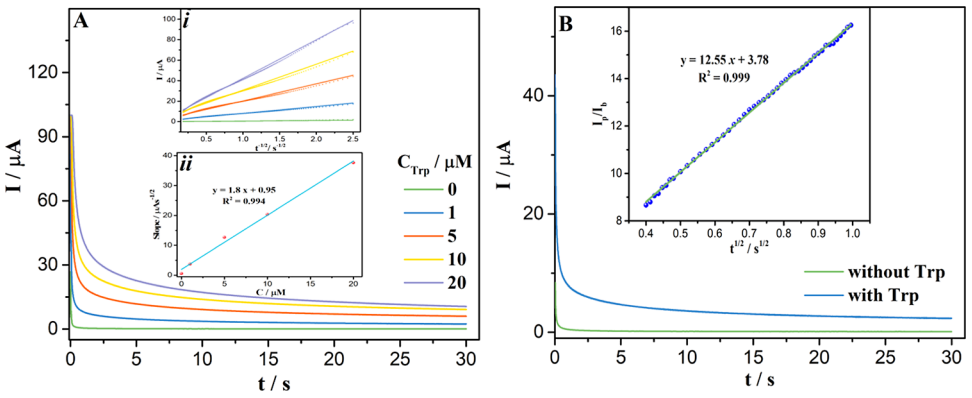

Figure 6. (A) CAs obtained at ND-CN550/GCE with the addition of different concentrations of Trp [inset: (i) plot I vs $t^{-1/2}$, (ii) plot of the slopes from (i) vs concentration of Trp]. (B) CAs obtained at ND-CN550/GCE with and without the addition of Trp (inset: I_p/I_b vs $t^{1/2}$ plot obtained from CA data) (measurements were made in triplicate and each point is the mean ± SD).

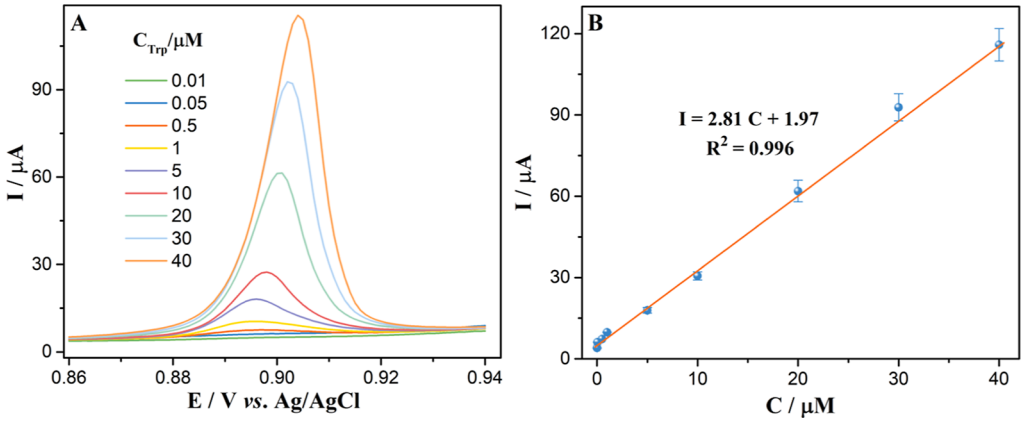

Figure 7. (A) SWV response for different concentrations of Trp at ND-CN550/GCE. (B) Calibration curve of Trp at ND-CN550/GCE at a pH of 3.0 (measurements were made in triplicate and each point is the mean ± SD).

second electron and proton (1e−, 1H+), which generates a cationic species [Structure (4) in Scheme 1]. Finally, the nucleophilic attack by Trp itself results in the formation the dimer [Structure (5) in Scheme 1].[34,36]

Effects of Scan Rate. The electrode process of Trp at ND-CN550/GCE was studied by examining the relationship between the oxidation current and scan rate. Figure 5 shows the effect of scan rate on the Trp oxidation current at ND-CN550/GCE. When the scan rate was increased from 10 to 100 mV/s, the anodic peak currents (I_{pa}) also increased (Figure 5A). The peak current value, as shown in Figure 5B,C, has a linear correlation with the square root of scan rates rather than the scan rates with a linear regression equation I (μA) = $1.92v^2 - 3.98$ (R^2 = 0.997) and I (μA) = $0.17v + 0.56$ (R^2 = 0.973), respectively. This suggests that the ND-CN550/GCE Trp oxidation reaction is a diffusion-controlled mechanism. Figure 5D shows a Tafel plot created with data from the CV Tafel area to obtain specific information about the rate-determining phase. The electron transfer coefficient (α) value of the electrodic reaction can be estimated from the Tafel slope using equation (eq 3).

$$E_p = \frac{b}{2}\log v + \text{constant} \tag{3}$$

Using the points of the Tafel area of the CV of Trp solution at the ND-CN550/GCE surface, the electron transfer coefficient (α) is calculated as 0.53, supposing a single electron transfer in the rate-determining phase between Trp and the ND-CN550/GCE surface.[37]

Reaction Kinetics for Oxidation of Trp at ND-CN550/GCE. The diffusion coefficients (D) and kinetic rate constant (K) of Trp at the ND-CN550/GCE were investigated using chronoamperometry (CA) in 0.1 M PBS (pH 3.0) at a potential of 1.2 V. The concentration of Trp CA evaluation was changed and is shown in Figure 6A. The Cottrell equation (eq 4) can be used to determine the diffusion coefficient (D) of Trp[38,39]

$$I_p = \frac{nFAC\sqrt{D}}{\sqrt{\pi t}} \tag{4}$$

where I_p stands for peak current (A), n is the number of electrons, F is the Faraday constant (96,500 C mol^{-1}), A is the electrode surface area (cm^2), C is the bulk concentration of the analyte (mol cm^{-3}), and t is the time (seconds). A linear relationship was obtained from the plot of I vs $t^{-1/2}$ of the CA measurements of different concentrations of Trp [inset (i) of Figure 6A]. After that, the slopes of I vs $t^{-1/2}$ of individual curves from inset (i) of Figure 6A were plotted against the concentration of Trp [inset (ii) Figure 6A]. As a result, the estimated value of D for Trp was 8.3×10^{-3} cm^2 s^{-1}.

Figure 6B depicts the CA response of ND-CN550/GCE in the absence and presence of Trp. The CA current response of Trp (I_p) is noticeably higher than the current response in the blank solution (I_b) at ND-CN550/GCE. The following

https://doi.org/10.1021/acsomega.3c06487
ACS Omega 2023, 8, 46869−46877

equation (eq 5) can be used to calculate the kinetic rate constant (K)[38]

$$\frac{I_p}{I_b} = (\pi KCt)^{1/2} \quad (5)$$

where I_p and I_b represent current with and without the addition of Trp, C represents the Trp concentration (mol cm^{-3}), t represents the time (seconds), and K is the reaction rate constant. A linear relationship was observed between the current ratio (I_p/I_b) and square roots of time. From the slope of I_p/I_b vs $t^{1/2}$, the calculated value of K was about 2.24×10^3 M^{-1} s^{-1}.

Effect of Temperature. The anodic current of Trp was studied in relation to the temperature at which ND-CN was produced. By raising the polymerization temperature to 550 °C, the oxidation current of Trp was increased; however, when the temperature was increased to 600 °C, the anodic current decreased (Figure S5). This might be because ND-CN contains the maximum number of defects, which gives the maximum anodic current of Trp. Therefore, a polymerization temperature of 550 °C was chosen as the optimal temperature for the synthesis of ND-CN for Trp detection.

Performance of the Developed Electrochemical Sensor for Trp Detection in Analytical Tests. The linear range and limit of detection (LOD) were investigated by using the SWV technique. Figure 7 depicts SWVs of varied Trp concentrations at the ND-CN550/GCE recorded under optimal experimental conditions. Trp oxidation current increases as the Trp concentration increases (Figure 7A). The anodic current of Trp at ND-CN550/GCE is proportional to Trp concentrations ranging from 0.01 to 40 μM (Figure 7B), with the following regression equation: I (μA) = 2.81C (μM) + 1.97, R^2 = 0.996. The LOD was calculated to be 0.0034 μM ($3\sigma/m$).

As shown in Table 1, the demonstrated electrochemical sensor has a promising analytical performance that is comparable to and better than those of previously described voltammetric methods for the detection of Trp.

Table 1. Comparison of Electrochemical Methods for Trp Determination

electrode	linear range (μM)	LOD (μM)	refs
Cs/Ce-MOF/GCE	0.25−331	0.14	9
tricobalt tetroxide/GCE	0.005−40	0.002	40
silver molybdate-reduced graphene oxide/GCE	0.02−146.96	0.0057	41
polythiophene−silver/GCE	0.2−400	0.02	42
copper oxide−poly L-glutamic acid/GCE	0.08−100	0.05	43
co-Ni-MOFs/GCE	0.01−100	0.0087	44
g-CN/GCE	−110	0.024	35
g-CN/CPE	0.1−120	0.085	45
SnSe/TiO_2@GO/GCE	0.0136−190	0.0053	46
ND-CN550/GCE	0.01−40	0.0034	this work

The presented electrochemical sensor exhibits promising analytical performance for the detection of Trp that is on par with or better than that of previously disclosed voltammetric approaches.

Repeatability, Reproducibility, and Effect of Interferences. To assess the repeatability of the ND-CN550/GCE, the oxidation current readings for 10 μM Trp were recorded for ten separate measurements, and the RSD was determined to be 3.02% (Figure S6A). Also, to examine the reproducibility of the method, three ND-CN550/GCEs were prepared in the same way. As shown in Figure S6B, an RSD of 5.97% for the determination of 10 μM Trp was obtained. As a result, we can conclude that the determination of Trp at ND-CN550/GCE had good repeatability and reproducibility. The effects of some selected interfering substances, including ascorbic acid (AA), dopamine (DA), uric acid (UA), L-cysteine (L-cys), L-arginine (L-arg), L-alanine (L-ala), and methionine (Meth) were studied on the determination of Trp. Figure S6C illustrates that the detection of Trp was found to be unaffected by selected interfering substances at concentrations 10 times greater than the concentration of Trp. This might be caused by different redox potentials of the selected species. Therefore, ND-CN550/GCE exhibits good selectivity for Trp detection.

Real Sample Analysis. The practical applicability of ND-CN550/GCE was assessed by using it for the detection of Trp in the cow's milk sample. The standard addition method was used to determine the content of Trp. Without any pretreatment, the milk was filtered and diluted 5-fold with 0.1 M PBS at pH 3.0. Also, the multivitamin tablets were ground and dissolved in double-distilled water. Then, the samples were centrifuged for 10 min to remove undissolved particles. Finally, the pH of the supernatant solution was adjusted to pH 3.0 with PBS.

Under the optimized experimental conditions, Trp in milk and multivitamin tablet samples was determined by spiking a standard Trp (1.0, 5.0, and 10.0 μM). As displayed in Table 2, satisfactory recoveries were obtained (97.8−108%); hence, the present method appears to be reliable and suitable for determining Trp in food samples. As a result, Trp may be accurately determined in real samples by using ND-CN550/GCE.

Table 2. Application of ND-CN550/GCE for Determination of Trp in Milk and Vitamin Tablets (n = 5)

sample	spiked	found	recovery %
milk	1.0	1.08	108.0
	5.0	4.89	97.8
	10.0	9.81	98.1
vitamin tablets	1.0	0.97	97.0
	5.0	5.31	106.2
	10.0	10.4	104.0

CONCLUSIONS

Finally, ultrathin ND-CN NSs were produced by using bulk ND-CN powders as a precursor by a simple ultrasonication process. The ND-CN NSs were used to build an electrochemical sensor for detecting Trp. Under optimal conditions, the ND-CN550/GCE demonstrated a better linear relationship with Trp concentrations ranging from 0.01 to 40 μM, with an LOD of 0.0034 μM. Furthermore, the demonstrated Trp sensor revealed good reproducibility, repeatability, and selectivity. Surface modification of g-CN by means of the introduction of defects enables ND-CN to possess superior electrochemical performance, which has an ultrathin structure for quick electron transport and a high surface area for interacting with targets. Lastly, the ND-CN550/GCE was used to detect Trp in real samples, and satisfactory findings were

https://doi.org/10.1021/acsomega.3c06487
ACS Omega 2023, 8, 46869−46877

obtained. As a result, ultrathin ND-CN NSs could be promising media for the development of sensitive electrochemical sensors.

■ ASSOCIATED CONTENT

Supporting Information

The Supporting Information is available free of charge at https://pubs.acs.org/doi/10.1021/acsomega.3c06487.

XPS survey of the synthesized materials, peak area ratio of N_2C and N_3C groups of *g*-CN and CN-NVs with different NV contents from XPS analysis, TEM images, the effect of the amount of ND-CN on the oxidation of Trp, effect of polymerization temperature, repeatability, reproducibility, and effect of interferences (PDF)

■ AUTHOR INFORMATION

Corresponding Author

Shimeles Addisu Kitte − *Department of Chemistry, College of Natural Sciences, Jimma University, 378 Jimma, Ethiopia;* orcid.org/0000-0001-8023-5165; Email: shimeles.addisu@ju.edu.et

Authors

Yeabsira Mihret − *Department of Chemistry, College of Natural Sciences, Jimma University, 378 Jimma, Ethiopia*

Getu Sisay − *Department of Chemistry, College of Natural Sciences, Jimma University, 378 Jimma, Ethiopia*

Abebe Diro − *Department of Chemistry, College of Natural Sciences, Jimma University, 378 Jimma, Ethiopia*

Solomon Hailemariam − *Department of Physics, College of Natural Sciences, Jimma University, 378 Jimma, Ethiopia*

Complete contact information is available at: https://pubs.acs.org/10.1021/acsomega.3c06487

Notes

The authors declare no competing financial interest.

■ ACKNOWLEDGMENTS

This study was supported by grants from Jimma University Research Council (project code: CNS-Chem-02-2022/23).

■ REFERENCES

(1) Zhang, Y.; Waterhouse, G. I. N.; Xiang, Z.; Che, J.; Chen, C.; Sun, W. A highly sensitive electrochemical sensor containing nitrogen-doped ordered mesoporous carbon (NOMC) for voltammetric determination of l-tryptophan. *Food Chem.* **2020**, *326*, 126976.

(2) Lima, D.; Andrade Pessôa, C.; Wohnrath, K.; Humberto Marcolino-Junior, L.; Fernando Bergamini, M. A feasible and efficient voltammetric sensor based on electropolymerized L-arginine for the detection of L-tryptophan in dietary supplements. *Microchem. J.* **2022**, *181*, 107709.

(3) He, Q.; Liu, J.; Feng, J.; Wu, Y.; Tian, Y.; Li, G.; Chen, D. Sensitive Voltammetric Sensor for Tryptophan Detection by Using Polyvinylpyrrolidone Functionalized Graphene/GCE. *Nanomaterials* **2020**, *10*, 125.

(4) Kałużna-Czaplińska, J.; Gątarek, P.; Chirumbolo, S.; Chartrand, M. S.; Bjørklund, G. How important is tryptophan in human health? *Crit. Rev. Food Sci. Nutr.* **2019**, *59*, 72−88.

(5) World Health Organization. Protein and amino acid requirements in human nutrition. *Report of a Joint WHO/FAO/UNU Expert Consultation*; WHO Press, 2007.

(6) Çevikkalp, S. A.; Löker, G. B.; Yaman, M.; Amoutzopoulos, B. A simplified HPLC method for determination of tryptophan in some cereals and legumes. *Food Chem.* **2016**, *193*, 26−29.

(7) Chen, G. N.; Lin, R. E.; Zhao, Z. F.; Duan, J. P.; Zhang, L. Electrogenerated chemiluminescence for determination of indole and tryptophan. *Anal. Chim. Acta* **1997**, *341*, 251−256.

(8) Altria, K. D.; Harkin, P.; Hindson, M. G. Quantitative determination of tryptophan enantiomers by capillary electrophoresis. *J. Chromatogr. B: Biomed. Sci. Appl.* **1996**, *686*, 103−110.

(9) Zhang, L.; Sun, M.; Jing, T.; Li, S.; Ma, H. A facile electrochemical sensor based on green synthesis of Cs/Ce-MOF for detection of tryptophan in human serum. *Colloids Surf., A* **2022**, *648*, 129225.

(10) Baranwal, J.; Barse, B.; Gatto, G.; Broncova, G.; Kumar, A. Electrochemical Sensors and Their Applications: A Review. *Chemosensors* **2022**, *10*, 363.

(11) Chimene, D.; Alge, D. L.; Gaharwar, A. K. Two-Dimensional Nanomaterials for Biomedical Applications: Emerging Trends and Future Prospects. *Adv. Mater.* **2015**, *27*, 7261−7284.

(12) Zhu, J.; Xiao, P.; Li, H.; Carabineiro, S. A. C. Graphitic Carbon Nitride: Synthesis, Properties, and Applications in Catalysis. *ACS Appl. Mater. Interfaces* **2014**, *6*, 16449−16465.

(13) (a) Hatamie, A.; Jalilian, P.; Rezvani, E.; Kakavand, A.; Simchi, A. Fast and ultra-sensitive voltammetric detection of lead ions by two-dimensional graphitic carbon nitride ($g\text{-}C_3N_4$) nanolayers as glassy carbon electrode modifier. *Measurement* **2019**, *134*, 679−687. (b) Ramalingam, M.; Ponnusamy, V. K.; Sangilimuthu, S. N. A nanocomposite consisting of porous graphitic carbon nitride nanosheets and oxidized multiwalled carbon nanotubes for simultaneous stripping voltammetric determination of cadmium(II), mercury(II), lead(II) and zinc(II). *Microchim. Acta* **2019**, *186*, 69.

(14) Ramalingam, M.; Ponnusamy, V. K.; Sangilimuthu, S. N. Electrochemical determination of 4-nitrophenol in environmental water samples using porous graphitic carbon nitride-coated screen-printed electrode. *Environ. Sci. Pollut. Res.* **2020**, *27*, 17481−17491.

(15) (a) Balasubramanian, P.; Settu, R.; Chen, S.-M.; Chen, T.-W. Voltammetric sensing of sulfamethoxazole using a glassy carbon electrode modified with a graphitic carbon nitride and zinc oxide nanocomposite. *Microchim. Acta* **2018**, *185*, 396. (b) Yan, Y.; Jamal, R.; Yu, Z.; Zhang, R.; Zhang, W.; Ge, Y.; Liu, Y.; Abdiryim, T. Composites of thiol-grafted PEDOT with N-doped graphene or graphitic carbon nitride as an electrochemical sensor for the detection of paracetamol. *J. Mater. Sci.* **2020**, *55*, 5571−5586.

(16) Huang, Y.; Tan, Y.; Feng, C.; Wang, S.; Wu, H.; Zhang, G. Synthesis of $CuO/g\text{-}C_3N_4$ composites, and their application to voltammetric sensing of glucose and dopamine. *Microchim. Acta* **2018**, *186*, 10.

(17) Fu, L.; Xie, K.; Wu, D.; Wang, A.; Zhang, H.; Ji, Z. Electrochemical determination of vanillin in food samples by using pyrolyzed graphitic carbon nitride. *Mater. Chem. Phys.* **2020**, *242*, 122462.

(18) Zhao, Z.; Sun, Y.; Dong, F. Graphitic carbon nitride based nanocomposites: a review. *Nanoscale* **2015**, *7*, 15−37.

(19) (a) Jiang, L.; Yuan, X.; Pan, Y.; Liang, J.; Zeng, G.; Wu, Z.; Wang, H. Doping of graphitic carbon nitride for photocatalysis: A review. *Appl. Catal., B* **2017**, *217*, 388−406. (b) Yu, H.; Shi, R.; Zhao, Y.; Bian, T.; Zhao, Y.; Zhou, C.; Waterhouse, G. I. N.; Wu, L.-Z.; Tung, C.-H.; Zhang, T. Alkali-Assisted Synthesis of Nitrogen Deficient Graphitic Carbon Nitride with Tunable Band Structures for Efficient Visible-Light-Driven Hydrogen Evolution. *Adv. Mater.* **2017**, *29*, 1605148.

(20) (a) Liao, J.; Cui, W.; Li, J.; Sheng, J.; Wang, H.; Dong, X. a.; Chen, P.; Jiang, G.; Wang, Z.; Dong, F. Nitrogen defect structure and NO+ intermediate promoted photocatalytic NO removal on H_2 treated $g\text{-}C_3N_4$. *Chem. Eng. J.* **2020**, *379*, 122282. (b) Liu, H.; Lei, W.; Tong, Z.; Li, X.; Wu, Z.; Jia, Q.; Zhang, S.; Zhang, H. Defect Engineering of 2D Materials for Electrochemical Energy Storage. *Adv. Mater. Interfaces* **2020**, *7*, 2000494.

(21) Zou, R.; Lin, Y.; Lu, C. Nitrogen Vacancy Engineering in Graphitic Carbon Nitride for Strong, Stable, and Wavelength Tunable Electrochemiluminescence Emissions. *Anal. Chem.* **2021**, *93*, 2678−2686.

(22) Kitte, S. A.; Bushira, F. A.; Xu, C.; Wang, Y.; Li, H.; Jin, Y. Plasmon-Enhanced Nitrogen Vacancy-Rich Carbon Nitride Electrochemiluminescence Aptasensor for Highly Sensitive Detection of miRNA. *Anal. Chem.* **2022**, *94*, 1406−1414.
(23) Niu, P.; Liu, G.; Cheng, H.-M. Nitrogen Vacancy-Promoted Photocatalytic Activity of Graphitic Carbon Nitride. *J. Phys. Chem. C* **2012**, *116*, 11013−11018.
(24) Yuan, J.; Liu, X.; Tang, Y.; Zeng, Y.; Wang, L.; Zhang, S.; Cai, T.; Liu, Y.; Luo, S.; Pei, Y.; et al. Positioning cyanamide defects in g-C_3N_4: Engineering energy levels and active sites for superior photocatalytic hydrogen evolution. *Appl. Catal., B* **2018**, *237*, 24−31.
(25) (a) Wei, W.; Yao, Y.; Zhao, Q.; Xu, Z.; Wang, Q.; Zhang, Z.; Gao, Y. Oxygen defect-induced localized surface plasmon resonance at the WO_{3-x} quantum dot/silver nanowire interface: SERS and photocatalysis. *Nanoscale* **2019**, *11*, 5535−5547. (b) Xue, D.; Xia, H.; Yan, W.; Zhang, J.; Mu, S. Defect Engineering on Carbon-Based Catalysts for Electrocatalytic CO_2 Reduction. *Nano-Micro Lett.* **2020**, *13*, 5.
(26) Yao, S.; Xue, S.; Peng, S.; Jing, M.; Qian, X.; Shen, X.; Li, T.; Wang, Y. Synthesis of graphitic carbon nitride at different thermal-pyrolysis temperature of urea and it application in lithium-sulfur batteries. *Mater. Sci.: Mater. Electron.* **2018**, *29*, 17921−17930.
(27) Wu, J.; Li, N.; Fang, H.-B.; Li, X.; Zheng, Y.-Z.; Tao, X. Nitrogen vacancies modified graphitic carbon nitride: Scalable and one-step fabrication with efficient visible-light-driven hydrogen evolution. *Chem. Eng. J.* **2019**, *358*, 20−29.
(28) Yu, H.; Shi, R.; Zhao, Y.; Bian, T.; Zhao, Y.; Zhou, C.; Waterhouse, G. I. N.; Wu, L.-Z.; Tung, C.-H.; Zhang, T. Alkali-Assisted Synthesis of Nitrogen Deficient Graphitic Carbon Nitride with Tunable Band Structures for Efficient Visible-Light-Driven Hydrogen Evolution. *Adv. Mater.* **2017**, *29*, 1605148.
(29) Wu, J.; Li, N.; Zhang, X.-H.; Fang, H.-B.; Zheng, Y.-Z.; Tao, X. Heteroatoms binary-doped hierarchical porous g-C_3N_4 nanobelts for remarkably enhanced visible-light-driven hydrogen evolution. *Appl. Catal., B* **2018**, *226*, 61−70.
(30) (a) Kang, Y.; Yang, Y.; Yin, L.; Kang, X.; Wang, L.; Liu, G.; Cheng, H. Selective Breaking of Hydrogen Bonds of Layered Carbon Nitride for Visible Light Photocatalysis. *Adv. Mater.* **2016**, *28*, 6471−6477. (b) Zhou, P.; Lv, F.; Li, N.; Zhang, Y.; Mu, Z.; Tang, Y.; Lai, J.; Chao, Y.; Luo, M.; Lin, F.; et al. Strengthening reactive metal-support interaction to stabilize high-density Pt single atoms on electron-deficient g-C3N4 for boosting photocatalytic H2 production. *Nano Energy* **2019**, *56*, 127−137. (c) Kang, Y.; Yang, Y.; Yin, L.; Kang, X.; Liu, G.; Cheng, H. An Amorphous Carbon Nitride Photocatalyst with Greatly Extended Visible-Light-Responsive Range for Photocatalytic Hydrogen Generation. *Adv. Mater.* **2015**, *27*, 4572−4577.
(31) Bushira, F. A.; Kitte, S. A.; Wang, Y.; Li, H.; Wang, P.; Jin, Y. Plasmon-Boosted Cu-Doped TiO2 Oxygen Vacancy-Rich Luminol Electrochemiluminescence for Highly Sensitive Detection of Alkaline Phosphatase. *Anal. Chem.* **2021**, *93*, 15183−15191.
(32) Cesiulis, H.; Tsyntsaru, N.; Ramanavicius, A.; Ragoisha, G. The Study of Thin Films by Electrochemical Impedance Spectroscopy. In *Nanostructures and Thin Films for Multifunctional Applications: Technology, Properties and Devices*; Tiginyanu, I., Topala, P., Ursaki, V., Eds.; Springer International Publishing, 2016; pp 3−42.
(33) Sundaresan, R.; Mariyappan, V.; Chen, S.-M.; Keerthi, M.; Ramachandran, R. Electrochemical sensor for detection of tryptophan in the milk sample based on MnWO4 nanoplates encapsulated RGO nanocomposite. *Colloids Surf., A* **2021**, *625*, 126889.
(34) Kim, S.; Sun, S.; Li, Y.; He, X. One-pot synthesis of graphene oxide coated with sol-gel for electrochemical determination of tryptophan. *Anal. Methods* **2015**, *7*, 6352−6359.
(35) Liu, X.; Zhang, J.; Di, J.; Long, Y.; Li, W.; Tu, Y. Graphene-like carbon nitride nanosheet as a novel sensing platform for electrochemical determination of tryptophan. *J. Colloid Interface Sci.* **2017**, *505*, 964−972.
(36) Radi, A.; Bekhiet, G. E. Voltammetry of melatonin at carbon electrodes and determination in capsules. *Bioelectrochem. Bioenerg.* **1998**, *45*, 275−279.
(37) Gholivand, M. B.; Pashabadi, A.; Azadbakht, A.; Menati, S. A nano-structured Ni(II)-ACDA modified gold nanoparticle self-assembled electrode for electrocatalytic oxidation and determination of tryptophan. *Electrochim. Acta* **2011**, *56*, 4022−4030.
(38) (a) Manavalan, S.; Ganesamurthi, J.; Chen, S.-M.; Veerakumar, P.; Murugan, K. A robust Mn@FeNi-S/graphene oxide nanocomposite as a high-efficiency catalyst for the non-enzymatic electrochemical detection of hydrogen peroxide. *Nanoscale* **2020**, *12*, 5961−5972. (b) Rajkumar, C.; Thirumalraj, B.; Chen, S.-M.; Veerakumar, P.; Liu, S.-B. Ruthenium Nanoparticles Decorated Tungsten Oxide as a Bifunctional Catalyst for Electrocatalytic and Catalytic Applications. *ACS Appl. Mater. Interfaces* **2017**, *9*, 31794−31805.
(39) Beitollahi, H.; Garkani-Nejad, F.; Tajik, S.; Ganjali, M. R. Voltammetric Determination of Acetaminophen and Tryptophan Using a Graphite Screen Printed Electrode Modified with Functionalized Graphene Oxide Nanosheets Within a Fe_3O_4@SiO_2 Nanocomposite. *Iran. J. Pharm. Res.* **2019**, *18*, 80−90.
(40) Zhao, D.; Lu, Y.; Ding, Y.; Fu, R. An amperometric L-tryptophan sensor platform based on electrospun tricobalt tetroxide nanoparticles decorated carbon nanofibers. *Sens. Actuators, B* **2017**, *241*, 601−606.
(41) Kokulnathan, T.; Chen, T.-W.; Chen, S.-M.; Kumar, J. V.; Sakthinathan, S.; Nagarajan, E. R. Hydrothermal synthesis of silver molybdate/reduced graphene oxide hybrid composite: An efficient electrode material for the electrochemical detection of tryptophan in food and biological samples. *Composites, Part B* **2019**, *169*, 249−257.
(42) GunaVathana, S. D.; Thivya, P.; Wilson, J.; Peter, A. C. Sensitive voltammetric sensor based on silver dendrites decorated polythiophene nanocomposite: Selective determination of L-Tryptophan. *J. Mol. Struct.* **2020**, *1205*, 127649.
(43) Khaleque, M. A.; Bacchu, M. S.; Ali, M. R.; Hossain, M. S.; Mamun, M. R. A.; Hossain, M. I.; Khan, M. Z. H. Copper oxide nanoflowers/poly-L-glutamic acid modified advanced electrochemical sensor for selective detection of L-tryptophan in real samples. *Heliyon* **2023**, *9*, No. e16627.
(44) Huang, W.; Chen, Y.; Wu, L.; Long, M.; Lin, Z.; Su, Q.; Zheng, F.; Wu, S.; Li, H.; Yu, G. 3D Co-doped Ni-based conductive MOFs modified electrochemical sensor for highly sensitive detection of L-tryptophan. *Talanta* **2022**, *247*, 123596.
(45) Abebe, H. A.; Diro, A.; Kitte, S. A. Voltammetric determination of tryptophan at graphitic carbon nitride modified carbon paste electrode. *Heliyon* **2023**, *9*, No. e21033.
(46) Eagambaram, M.; Kumar, K. Design of an Efficient Tin Selenide-Based Ternary Nanocomposite Electrode for Simultaneous Determination of Paracetamol, Tryptophan, and Caffeine. *ACS Omega* **2022**, *7*, 35486−35495.

https://doi.org/10.1021/acsomega.3c06487
ACS Omega 2023, 8, 46869−46877